ELSEVIER

www.elsevier.nl/locate/jorganchem

Journal of Organometallic Chemistry 616 (2000) 10–18

Journal of Organometallic Chemistry

Synthetic, structural, and dynamic NMR studies of (bisphosphine)palladium(0) complexes of dibenzylideneacetone

Steven M. Reid, Joel T. Mague, Mark J. Fink *

Department of Chemistry, Percival Stern Hall, Tulane University, New Orleans, LA 70118-5698, USA

Received 25 April 2000; received in revised form 7 July 2000

Abstract

Two complexes of the type $(R_2PCH_2CH_2PR_2)Pd(dba)$ have been prepared by the reaction of $Pd_2(dba)_3{\cdot}CHCl_3$ with $R_2PCH_2CH_2PR_2$ (R = ^{i}Pr (**1**), 74%; Cy (**2**), 57%; dba = dibenzylideneacetone). X-ray crystallographic studies of **1** and **2** reveal that the coordinated dba ligand adopts an *s-trans*, *s-trans* conformation in which the palladium is coordinated to one C=C bond in an η^2-fashion. Variable temperature, ^{1}H- and ^{31}P{H}-NMR spectroscopy of **1** show two distinct dynamic processes in solution. In the ^{1}H-NMR spectra, a rapid intramolecular exchange of coordinated and uncoordinated C=C bonds is observed with the estimated $\Delta G^{\ddagger}_{ex}$ being 14 kcal mol^{-1}. In the ^{31}P{H}-NMR spectra, a facile interconversion of the predominant *s-trans*, *s-trans* conformer with the minor *s-trans*, *s-cis*, and *s-cis*, *s-cis* conformers begins to occur at higher temperatures. Molecular mechanics calculations place the relative energies of the three isomers at 0, 0.9, and 4.7 kcal mol^{-1}, respectively. An intramolecular mechanism for double bond exchange is proposed to occur via a symmetric transition state involving the *s-cis*, *s-cis* conformer. Strong coordination of dba to palladium in **1** is proposed to account for slow reactions with PhX where the relative rates of oxidative addition were found to increase in the order of X = Cl ≪ Br < I.

Keywords: Palladium; Dibenzylideneacetone; X-ray; Intramolecular exchange

1. Introduction

Coordinatively unsaturated and zero-valent palladium fragments of the types $(P)_2Pd$ and (P–P)Pd are generally accepted as the active catalytic species in many kinds of reactions (P = monodentate phosphine; P–P = chelating bisphosphine) [1]. Convenient sources of palladium(0) in these reactions are the air-stable complexes $Pd_2(dba)_3{\cdot}CHCl_3$ and $Pd(dba)_2$ (dba = dibenzylideneacetone) [2,3]. The mechanism of the in situ formation of dba-stablilized complexes (P–P)Pd(dba) has been established by Amatore and Jutand for a variety of mono- and bidentate-phosphines (Scheme 1) [4–6]. This mechanism was found to be operative for reaction mixtures that contain $Pd(dba)_2$ and one equivalent of a bisphosphine P–P that bears aryl substituents on phosphorus to afford complexes of the type $(P–P)_2Pd$. Subsequent redistribution with Pd(dba) eventually generates (P–P)Pd(dba) [7].

$$2Pd(dba)_2 \longrightarrow 2Pd(dba) + 2dba$$

$$2Pd(dba) + 2P\text{-}P \longrightarrow Pd(dba) + Pd(P\text{-}P)_2 + dba$$

$$Pd(dba) + Pd(P\text{-}P)_2 + dba \longrightarrow 2(P\text{-}P)Pd(dba)$$

Scheme 1.

The burgeoning utility of palladium sources such as $Pd_2(dba)_3{\cdot}CHCl_3$ in catalytic reactions has sparked an increasing number of investigations of isolated complexes (P–P)Pd(dba) and $(P)_2Pd(dba)$. An early report by Pierpont et al. [8] described the X-ray crystal structure of (bipy)Pd(dba) which appears to be the first structurally characterized example of molecules of the type $L_2Pd(dba)$ (bipy = 2,2′-bipyridine) [9]. More recent examples include related complexes that contain chelating [10–15] and monodentate [16,17] ancillary ligand motifs.

Previous studies of zero-valent palladium complexes in this laboratory led to the discovery of $[(dcpe)Pd]_2$ which furnishes the highly reactive (dcpe)Pd(0) fragment through a rapid dimer-monomer equilibrium

* Corresponding author. Fax: +1-504-8655596.
E-mail address: fink@tulane.edu (M.J. Fink).

0022-328X/00/$ - see front matter
PII: S0022-328X(00)00524-6

(dcpe = 1,2-bis(dicyclohexylphosphino)ethane) [18]. The limiting small scale synthesis of this complex together with its instability toward oxygen and water prompted us to pursue a more straightforward and practical route to (P–P)Pd(0) from related complexes (P–P)Pd(dba). Herein we describe the synthesis and X-ray crystal structures of two such species containing electron-rich chelating bisphosphines. Additionally, we report a dynamic NMR study on one of these complexes.

2. Results

2.1. Synthesis

Slow addition of dippe or dcpe to a dark purple solution of $Pd_2(dba)_3{\cdot}CHCl_3$ in benzene gradually gave an orange solution of (dippe)Pd(dba) (**1**) or an orange precipitate of (dcpe)Pd(dba) (**2**) as shown in Eq. (1)

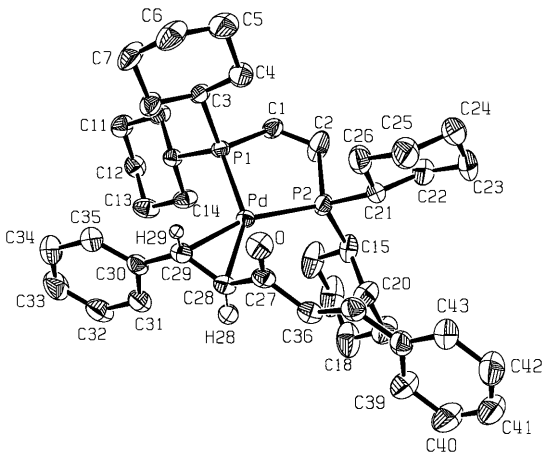

Fig. 1. ORTEP view and atom numbering scheme of **1**. Most hydrogen atoms have been omitted for clarity. Thermal ellipsoids are drawn at the 30% probability level.

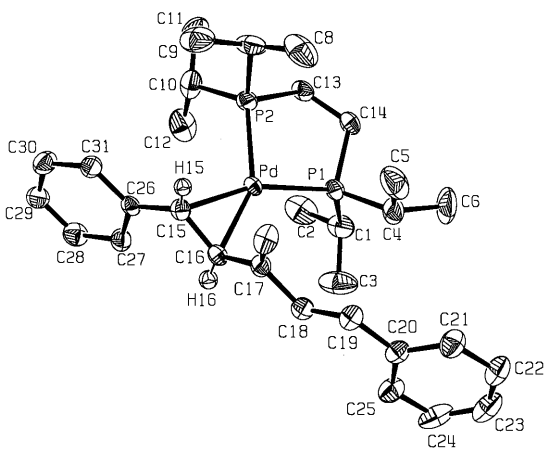

Fig. 2. ORTEP view and atom numbering scheme of **2**. A molecule of $CH_2Cl_2$and most hydrogen atoms have been omitted for clarity. Thermal ellipsoids are drawn at the 30% probability level.

(dippe = 1,2-bis(diisopropylphosphino)ethane). Large orange crystals of **1** were obtained in 74% yield from cold benzene–pentane at −20°C whereas complex **2** was isolated as dark red–orange cubes in 57% yield from cold CH_2Cl_2–Et_2O.

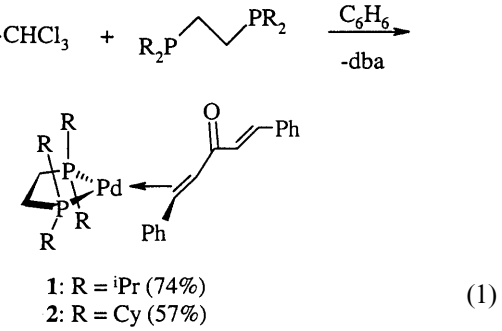

(1)

The dippe derivative **1** decomposes in air over several months and much more rapidly (1–2 days) in hydrocarbon solution. Even more rapid decomposition was observed in $CDCl_3$ and CD_2Cl_2 to give unidentifiable products ($^{31}P\{H\}$-NMR). In contrast, the more sterically congested **2** was found to be more robust and could be manipulated under air and in chlorinated solvents for short periods of time without appreciable decomposition. ^{1}H-NMR spectra of **1** (C_6D_6) and **2** (toluene-d_8) at 20°C each reveal broad resonances including those for one coordinated dba ligand while the $^{31}P\{H\}$-NMR spectra each consist of two broad resonances of equal intensity. The origin of these broad resonances will be discussed in a later section.

2.2. X-ray crystallography

The solid state structures of **1** and **2** were determined by X-ray crystallography. ORTEP views of **1** and **2** are given in Figs. 1 and 2, respectively, while experimental details and relevant metrical data for both complexes are presented in Tables 1–3. A comparison of bond angles and distances in **1** and **2** indicates that the core geometries of their structures are virtually superimposable while minor differences between the two are not statistically significant. The bond distances of the coordinated olefins (1.428(8) Å for **1** and 1.408(7) Å for **2**) are significantly shorter than those observed for the related (dppe)Pd(dba) (1.522(8) Å) [10] and $[(Cy_2PCH_2)_2NMe]$Pd(dba) (1.52(3) Å) [12] but comparable to those in [2-(2′-dicyclohexylphosphinophenyl)-2-methyl-1,3-dioxolane]Pd(dba) (1.423(3) Å) [11], $[P(Ph_2Np)_3]_2$Pd(dba) (1.44(3) Å) and $(PBz_3)_2$Pd(dba) (1.45(4) Å) [16], and both molecules of (2,2′-bipyridine)Pd(dba) (1.42(1) and 1.45(1) Å) [8]. In accordance with structural data for the five complexes that contain symmetrical ancillary ligand arrays mentioned above, there is no statistical difference between both Pd–C_{olefin} bond distances in either **1** or **2**. The only

exception to this trend appears to be [$(Cy_2PCH_2)_2$-NMe]Pd(dba) for which a weak Pd···$O_{carbonyl}$ interaction was proposed to shorten one Pd–C_{olefin} bond (Pd–O = 3.296 Å). The corresponding Pd···$O_{carbonyl}$ distance in **1** is 3.293 Å and in **2** is 3.177 Å but we find no clear evidence of Pd···$O_{carbonyl}$ interactions in either complex. The C15–C16–P1–P2 torsion angle in **1** (1.5°) and C28–C29–P1–P2 torsion angle in **2** (2.8°) indicate only slight twists between each set of ligand manifolds. The P1–Pd–P2 bite angles in **1** (88.26(5)°) and **2** (88.04(5)°) are similar to that observed previously for (dppe)Pd(dba) (87.19(5)°).

Table 1
Crystal data and structure refinement for **1** and **2**

Compound	(dippe)Pd(dba) (**1**)	(dcpe)Pd(dba)·CH_2Cl_2 (**2**)
Color/shape	Orange/column	Orange/block
Chemical formula	$C_{31}H_{46}OP_2Pd$	$C_{44}H_{64}Cl_2OP_2Pd$
Temperature (K)	293(2)	293(2)
Crystal system	Orthorhombic	Triclinic
Space group	$Pna2_1$	$P\bar{1}$
Unit cell dimensions		
a (Å)	21.470(1)	12.017(1)
b (Å)	8.6569(8)	19.751(1)
c (Å)	17.193(2)	9.5524(9)
α (°)		95.515(6)
β (°)		99.598(8)
γ (°)		77.948(6)
V (Å^3)	3195.7(5)	2181.7(3)
Z	4	2
D_{calc} (g cm^{-3})	1.253	1.291
Absorption coefficient (mm^{-1})	0.701	0.652
Radiation	Mo–K_α ($\lambda = 0.71073$)	Mo–K_α ($\lambda = 0.71073$)
Diffractometer/scan type	Enraf–Nonius CAD4/$\theta/2\theta$	Enraf–Nonius CAD4/$\theta/2\theta$
θ Range for data collection (°)	1.90–25.98	1.75–25.24
Reflections measured	3242	8170
Independent/observed reflections	3242/2663 [$I > \sigma 2(I)$]	7765/4491 [$I > \sigma 2(I)$]
Data/restraints/parameters	3242/1/332	7765/0/459
Extinction coefficient	None	None
Goodness-of-fit on F_2	1.045	1.007
Final R indices [$I > \sigma 2(I)$]	$R_1 = 0.0247$, $wR_2 = 0.0604$	$R_1 = 0.0437$, $wR_2 = 0.0952$
R indices (all data)	$R_1 = 0.0466$, $wR_2 = 0.0652$	$R_1 = 0.1508$, $wR_2 = 0.1165$

Table 2
Selected bond lengths (Å) and angles (°) for **1**

Bond lengths	
Pd–P(1)	2.310(1)
Pd–P(2)	2.282(1)
Pd–C(15)	2.151(4)
Pd–C(16)	2.148(4)
P(1)–C(14)	1.838(5)
P(2)–C(13)	1.853(5)
C(15)–C(16)	1.428(8)
C(13)–C(14)	1.528(7)
Bond angles	
C(15)–Pd–C(16)	38.8(2)
P(1)–Pd–P(2)	88.26(5)
P(1)–Pd–C(15)	160.9(2)
P(2)–Pd–C(16)	149.5(1)
P(1)–Pd–C(16)	122.1(1)
P(2)–Pd–C(15)	110.8(2)

Table 3
Selected bond lengths (Å) and angles (°) for **2**

Bond lengths	
Pd–P(1)	2.283(1)
Pd–P(2)	2.307(1)
Pd–C(28)	2.159(5)
Pd–C(29)	2.159(5)
P(1)–C(1)	1.852(5)
P(2)–C(2)	1.863(5)
C(28)–C(29)	1.408(7)
C(1)–C(2)	1.406(7)
Bond angles	
C(28)–Pd–C(29)	38.1(2)
P(1)–Pd–P(2)	88.04(5)
P(2)–Pd–C(29)	162.0(1)
P(1)–Pd–C(28)	147.9(2)
P(2)–Pd–C(28)	124.0(2)
P(1)–Pd–C(29)	109.9(2)

2.3. Reactions between *1* and halobenzenes

It is generally accepted that a key step in many palladium catalyzed reactions that involve aryl halides (or pseudo-halides) is the oxidative addition of ArX to $L_2Pd(0)$ species to furnish intermediates of the type $L_2Pd(Ar)X$. Although it would be more convenient in practice to generate such intermediates from mixtures of $Pd_2(dba)_3$ (or $Pd(dba)_2$) and phosphines L, we undertook a brief survey of reactions between isolated **1** and PhX in order to assess the relative ease with which oxidative additions to **1** proceed in the absence of excess dba (X = Cl, Br, I). As depicted in Eq. (2), **1** was treated with five equivalents of PhX in toluene-d_8 at 65°C and then monitored by ^{1}H- and ^{31}P{H}-NMR. No reaction was observed for X = Cl, even after five days. The reaction of **1** with PhBr, however, was judged to be complete after five days to give (dippe)Pd(Ph)Br (**3a**) and that with PhI after 72 h to give (dippe)Pd(Ph)I (**3b**), therefore leading us to assign relative reactivities of PhX in the order Cl ≪ Br < I. The ^{1}H-NMR spectra of reaction mixtures containing **3a** and **3b** are similar and each shows resonances for one equivalent of free dba. Additionally, inequivalent methylene protons in the PCH_2CH_2P backbone give rise to two multiplets; similar patterns are observed for the dippe methyne protons.

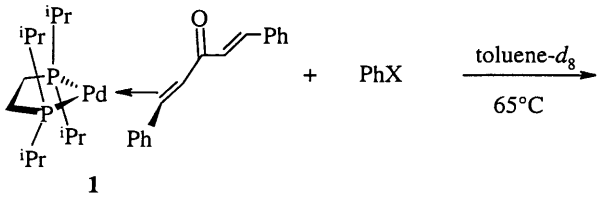

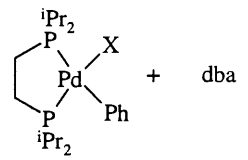

3a: X = Br
3b: X = I (2)

Four clearly resolved doublet of doublets between δ 0.7 and 1.4 indicate four magnetically inequivalent sets of dippe methyl groups as would be expected for square planar complexes of C_s point symmetry as shown in Eq. (2). The $^{31}P\{H\}$-NMR spectra of **3a** and **3b** are also similar in that they are each comprised of an AB pattern of doublets at δ 68.58 and 75.48 ($J_{PP} = 19$ Hz) for **3a** and δ 68.08 and 72.43 ($J_{PP} = 18$ Hz) for **3b**. The values of these coupling constants J_{PP} are considerably less than those reported by Amatore et al. for a range of complexes (P–P)Pd(Ph)I that contain chelating phosphines less basic than dippe [7].

2.4. Dynamic NMR studies of *1*

The observation of broad resonances in the ^1H- and $^{31}P\{H\}$-NMR spectra of **1** and **2** at 20°C suggested dynamic behavior of **1** and **2** in solution. The low solubility of **2** in hydrocarbon solvents (e.g. C_6D_6 and toluene-d_8) precluded variable temperature NMR spectra of this complex in solution; however, detailed NMR studies on the more soluble **1** was possible. The 400.08 MHz ^1H-NMR spectrum of **1** in toluene-d_8 at -80°C shows two different sets of olefinic resonances for the dba ligand (Fig. 3). Two well-resolved doublets at δ 7.34 and 8.06 ($J_{HH} = 15$ Hz) correspond to the protons of one uncoordinated double bond of dba. Two complex resonances at δ 5.13 and 5.84 are attributed to the protons of a double bond coordinated to palladium. Inequivalent phenyl groups on the dba ligand give rise to two separate resonances for each set of *ortho* (δ 7.40 and 7.50) and *meta* (δ 7.14 and 7.21) protons while the *para* protons give rise to two overlapping resonances at δ 7.01. Each dippe methyl group is evidently rendered magnetically inequivalent as is evidenced by eight sets of partially resolved and overlapping doublets of doublets that in turn obscure resonances from the PCH_2CH_2P ligand backbone. Additionally, inequivalent $CHMe_2$ protons give rise to two multiplets at δ 1.41 and 1.89, respectively, in a 3:1 ratio.

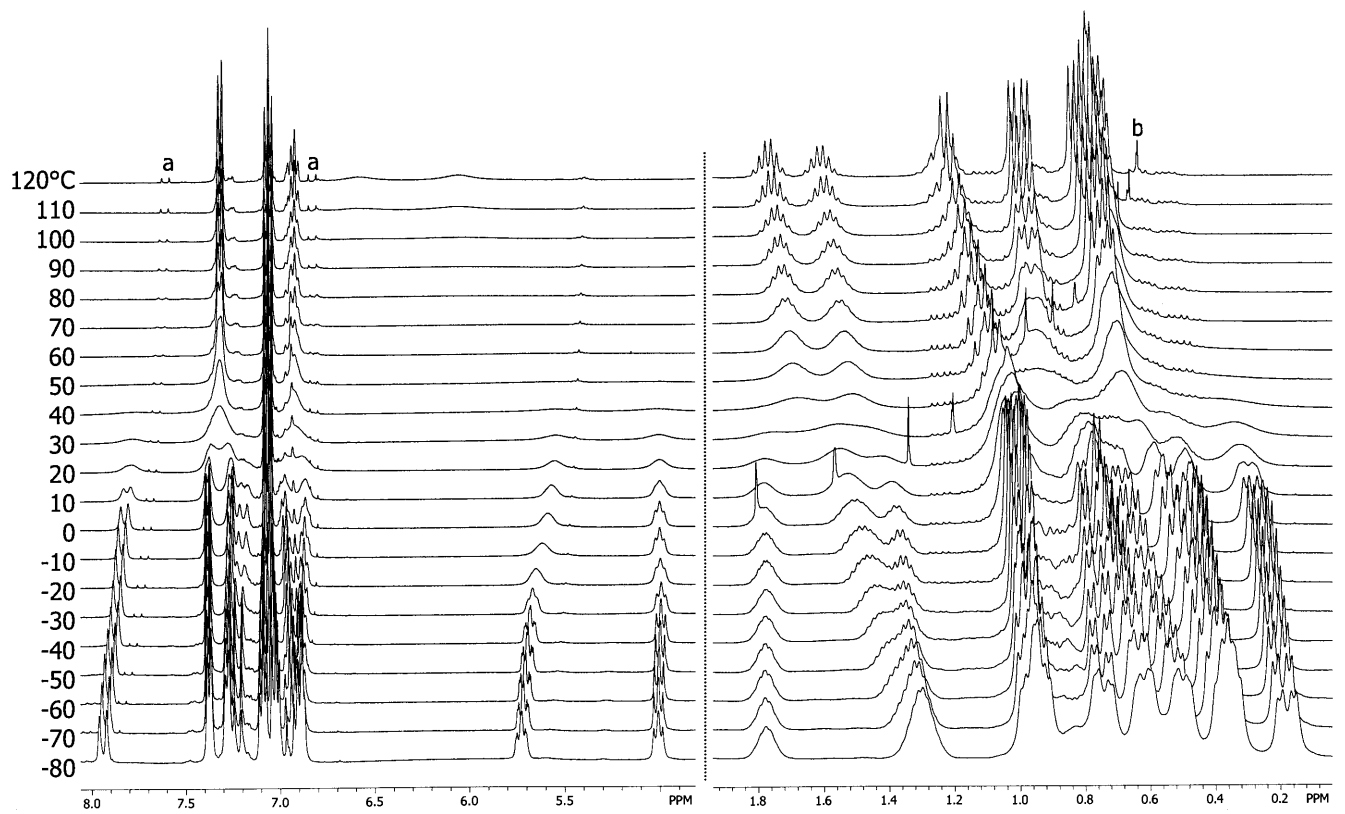

Fig. 3. ^1H-NMR (400.08 MHz) variable temperature spectra of **1** in toluene-d_8. [a]Free dba; [b]solvent impurity.

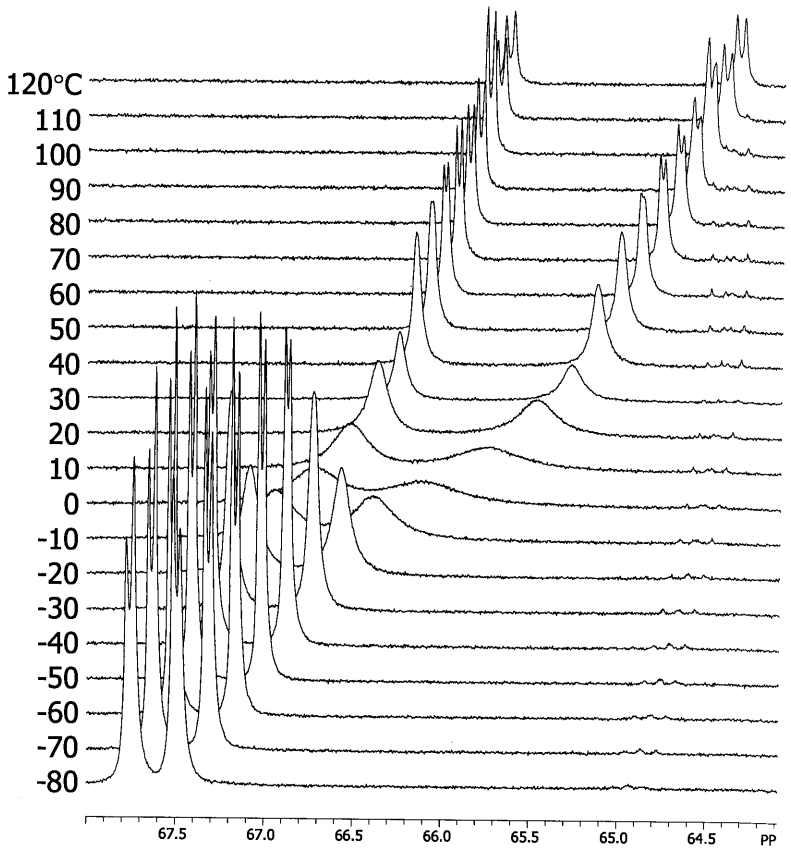

Fig. 4. $^{31}P\{H\}$-NMR (161.96 MHz) variable temperature spectra of **1** in toluene-d_8. Not shown on the figure is a very weak AB pattern centered at 62.4 ppm. It is only observed at temperatures below -30°C, and is attributed to the minor ($\leq 1\%$) *s-cis*, *s-trans* conformer of **1.**

The 161.96 MHz $^{31}P\{H\}$-NMR spectrum at -80°C consists primarily of a well-resolved AB pattern ($\delta =$ 67.75 and 67.49; $J_{PP} = 6.43$ Hz). Close inspection of the baseline revealed the presence of a minor component (ca. 1%) that gave rise to another AB pattern (δ 63.82 and 60.86; $J_{PP} = \sim 9$ Hz). Both the low temperature ^1H- and $^{31}P\{H\}$-NMR data are consistent with coordination of dba to palladium through one olefinic bond representative of a primarily static solution structure of **1** similar to that found in the solid state (Fig. 1).

When the temperature was raised, the ^1H- and $^{31}P\{H\}$-NMR spectra indicated that **1** exhibits dynamic behavior in solution. As Fig. 3 indicates, the sharp olefinic resonances of the dba ligand at -80°C gradually broadened as the sample was warmed and finally coalesced at 20°C. Upon further warming to 120°C, a single set of two broad olefinic resonances gradually emerged at δ 6.59 and 6.46. These chemical shifts are the approximate arithmetic means of those for the protons of the uncoordinated and coordinated dba double bonds, respectively, in the -80°C spectrum. Resonances from the dba phenyl groups also coalesced to give one set of sharp *ortho*, *meta*, and *para* proton signals at 120°C. Furthermore, the 120°C spectrum shows that the dippe ligand resonances consist of two sets of overlapping methyl doublets of doublets while the C*H*Me$_2$ protons give rise to two well-resolved multiplets at δ 1.62 and 1.77. A single multiplet for the PCH_2CH_2P backbone appeared at δ 1.23.

Results from the corresponding variable temperature $^{31}P\{H\}$-NMR experiment are presented in Fig. 4. The sharp AB pattern of the major species in the -80°C $^{31}P\{H\}$-NMR spectrum of **1** was preserved up to -30°C above which it gradually collapsed to give two increasingly broad resonances of equal intensity. Analogous behavior (not shown in Fig. 4) was also observed for the AB pattern of the minor species. One AB pattern then reemerged at 60°C and remained relatively unchanged up to 120°C, whereas no minor component was observed at all above -30°C. As shown in Fig. 4, the chemical shifts of the major species at -80°C simultaneously diverged and shifted slightly upfield with increasing temperature.

3. Discussion

A correct interpretation of the dynamic NMR behavior of **1** in solution must take into account two distinct processes: the facile interconversion of the rotational

isomers of the complex, and the exchange between coordinated and free olefins of the dba ligand. The variable temperature ^{1}H-NMR data are consistent with an intramolecular exchange of coordinated and uncoordinated dba double bonds as shown in Scheme 2. We have ruled out any intermolecular mechanism that involved dba since a trace impurity of free dba gave rise to sharp ^{1}H signals that did not coalesce over the temperature range of this experiment.

The ground state *s-trans*, *s-trans* conformer I is that observed in the solid state. Successive rotations by 180° about each $C_{carbonyl}$–C(H)C(Ph) single bond would give *s-cis*, *s-trans* conformer II followed by the *s-cis*, *s-cis* conformer III. Early structural work on dba complexes of palladium demonstrated that the dba ligands may adopt both *s-cis*, *s-trans* and *s-cis*, *s-cis* conformers in the solid state [3,19–21], a fact that was confirmed by a more recent and accurate determination of the structure of $Pd_2(dba)_3{\cdot}CH_2Cl_2$ [14]. The exchange of coordinated and uncoordinated dba double bonds is proposed to occur from the *s-cis*, *s-cis* conformer via the transition state IV in which the geometry about palladium is pseudo-tetrahedral. This is similar to the low energy configuration observed in the X-ray crystal structure of (dcpe)Ni(η^4-C_4H_6) [22]. This mechanism nicely accommodates the fact that the two phosphorus nuclei remain inequivalent over the entire temperature range of the variable temperature NMR experiments.

The significant number of exchanging spins observed in the ^{1}H-NMR spectra rendered full lineshape analysis too computationally complex. Consequently, the free energy of activation for this exchange process $\Delta G^{\ddagger}_{ex}$ was estimated from the coalescence temperature ($\sim$20°C; Fig. 3) for the aromatic *ortho* protons that yielded a value of $\sim$14 kcal mol^{-1}. This is greater than the estimated values for double bond exchange in (^{t}Bu$_2$PCH$_2$CH$_2$P^{t}Bu$_2$)Pd(C_4H_6) ($\Delta G^{\ddagger}_{ex}$ = 12 kcal mol^{-1}; solid state) [22] and (^{t}Bu$_2$PCH$_2$CH$_2$P^{t}Bu$_2$)Ni(C_4H_6) ($\Delta G^{\ddagger}_{ex}$ = 7–8 kcal mol^{-1}; solution) [23].

The mechanism in Scheme 2 is analogous to that proposed by Jolly et al. for trigonal planar complexes of the type ($R_2PCH_2CH_2PR_2$)Pd(η^2-C_4H_6) in which intramolecular exchange of coordinated and uncoordinated butadiene double bonds was observed both in solution [24] and in the solid state (R = Cy, ^{i}Pr, ^{t}Bu) [22]. The same mechanism was invoked to explain similar double bond exchange phenomena in (^{t}Bu$_2$PCH$_2$CH$_2$P^{t}Bu$_2$)Ni(C_4H_6) [23] and ($R_2PCH_2CH_2PR_2$)Pd(1,5-C_6H_{10}) [25] although in these examples exchange of the phosphorus nuclei was also observed at higher temperatures (R = ^{i}Pr, ^{t}Bu).

The changes in lineshape in the variable temperature ^{31}P{H}-NMR reflect a second process — quite distinct from the double bond exchange discussed above — involving rapid interconversion of the conformers shown in Scheme 2. Molecular mechanics calculations on **1** confirmed the presence of I, II, and III as local minima on the conformational potential energy surface with relative energies of 0, 0.9, and 4.7 kcal mol^{-1}, respectively. The rotational barrier for I→II was estimated to be 5 kcal mol^{-1} and that for II→III was estimated to be 7.4 kcal mol^{-1}. These values are consistent with the tentative assignment to II as the minor component in the −80°C ^{31}P{H}-NMR spectrum. At higher temperatures, however, the population of intermediates II and III would be expected to increase, but so would the rates of exchange between those species, therefore precluding any spectral assignments to intermediates other than II. For this reason it was impossible to accurately analyze conformer equilibria from ^{31}P{H}-NMR spectra by computer simulation. We note, however, that the observed change in lineshapes and chemical shifts with increasing temperature are qualitatively consistent with increasing populations of conformers II and III.

The relatively slow reactions of **1** with PhI and especially PhBr in toluene at elevated temperatures are

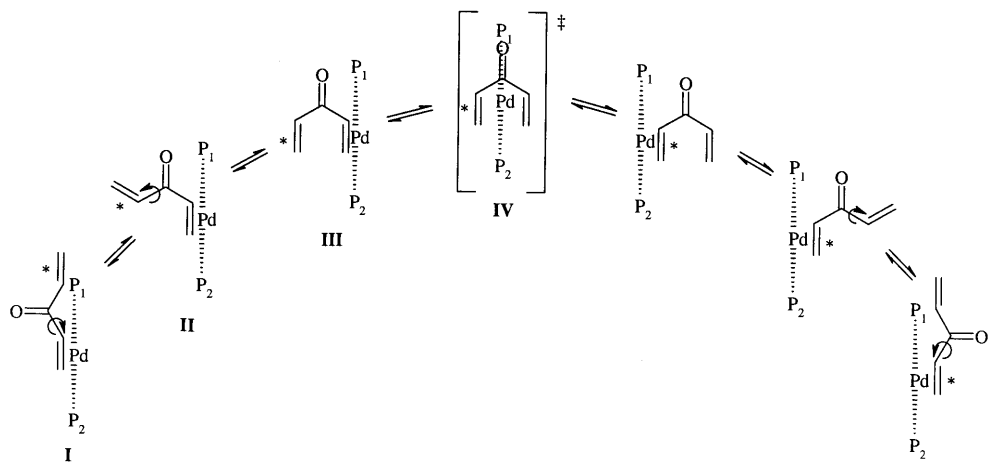

Scheme 2. Proposed intermolecular exchange of coordinated and uncoordinated double bonds in **1** (phenyl groups have been omitted for clarity).

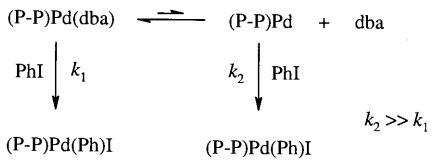

Scheme 3.

the likely consequences of dba being tightly bound to palladium. Dissociation of dba from $L_2Pd(dba)$ to give a highly reactive 14 electron species $L_2Pd(0)$ is generally accepted to occur before the oxidative addition of PhX to palladium [6]. A facile equilibrium involving free dba and (dippe)Pd(0) is clearly not observed for **1** on the NMR time scale, although we cannot rule out the possibility that it occurs on the chemical time scale. Amatore et al. have studied the kinetics of oxidative addition of PhI to (P–P)Pd(dba) (P–P = DIOP, dppf, or BINAP). The overall reaction rates were dependent both on the position of the dissociative equilibria and the relative rates of reaction of PhI with (P–P)Pd(dba) and (P–P)Pd(0) (Scheme 3). As expected, (P–P)Pd(0) was found to be the most reactive species towards PhI; however, reaction with (P–P)Pd(dba) does occur but with rates several orders of magnitude less than those for (P–P)Pd(0) [7]. In contrast, Pregosin et al. demonstrated that other complexes of the type (P–P)Pd(dba) do not undergo oxidative addition with PhI at all, even after prolonged reaction times. The authors concluded that the presence of dba could be detrimental to catalytic reactions in which bidentate ligands are employed [26]. Our qualitative results are consistent with the mechanism presented in Scheme 3. The overall reactivity of (dippe)Pd(0) should be high towards PhI and PhBr [27]; therefore, the low reactivity of **1** towards these halobenzenes is the likely consequence of the extremely low availability of (dippe)Pd(0) from the dissociation equilibrium.

4. Conclusion

We have prepared two examples of air-stable complexes of the type (P–P)Pd(dba). The X-ray crystal structures of both are in general agreement with the limited number of other structurally characterized palladium(0) complexes of dba. However, dynamic ^{1}H- and ^{31}P{H}-NMR studies revealed that **1** is the first example in which a dba ligand has been shown to undergo temperature dependent intramolecular double bond and conformer exchanges, respectively, particularly to the exclusion of any observable intermolecular exchange processes. For this latter reason, the reaction of **1** with halobenzenes is prohibitively slow to be of practical significance. While oxidative additions of PhX to (P–P)Pd(0) fragments are generally conceded to occur more rapidly with increasing basicity of the bisphosphine, our studies suggest that this trend can be substantially attenuated when dba is present as a coordinating ligand.

5. Experimental

5.1. General procedures and instrumentation

All air-sensitive manipulations were conducted under an atmosphere of dry argon in oven-dried glassware using standard Schlenk techniques. Benzene, Et_2O, and pentane were freshly distilled from purple sodium benzophenone ketyl just prior to use. Other solvents were of reagent grade and used without further purification. C_6D_6 and toluene-d_8 were dried over sodium benzophenone ketyl and then transferred via vacuum transfer into either storage flasks containing 4 Å molecular sieves or directly into NMR tubes. Chlorobenzene, bromobenzene, and iodobenzene were distilled from CaH_2 under Ar and stored over 4 Å molecular sieves. 1,2-bis(dicyclohexylphosphino)ethane (dcpe) was purchased from Strem Chemicals, Inc. 1,2-bis(diisopropylphosphino)ethane (dippe) [28] and $Pd_2(dba)_3{\cdot}CHCl_3$ [2,3] were prepared according to published procedures.

NMR spectra were acquired on a GE Omega 400 MHz spectrometer with the following operating frequencies: ^{1}H- (400.08 MHz), ^{31}P{H}-(161.96 MHz). Chemical shifts are reported in ppm and coupling constants in hertz. All spectra were acquired at ca. 20°C unless otherwise noted. Elemental analyses were performed by Schwarzkopf Micoanalytical Laboratory, Inc. (Woodside, NY).

5.2. Preparations

5.2.1. (dippe)Pd(dba) (*1*)

A stirred dark purple solution of $Pd_2(dba)_3{\cdot}CHCl_3$ in 30 ml C_6H_6 was treated dropwise with neat dippe (760 mg, 2.90 mmol). The solution gradually changed to orange and was stirred for a total of 15 min, then concentrated to $\sim$10 ml. Et_2O (15 ml) and pentane (15 ml) were added to precipitate free dba which was allowed to settle and the mother liquor was siphoned into another flask and stripped to dryness. The resulting crude product was crystallized from C_6H_6–pentane at 0°C as orange crystals that were washed once with pentane and dried in vacuo; yield 1.289 g (74%). ^{1}H-NMR (C_6D_6): δ 0.3–2.0 (br, 36, dippe), 5.16 (br, 1, HC=CH), 5.73 (br, 1, HC=CH), 6.9–7.6 (br, 11, Ph and HC=CH), 8.02 (br, 1, HC=CH). ^{31}P{H}-NMR (C_6D_6): δ 65.83 (br, 1), 66.67 (br, 1). Anal. Calc. for $C_{31}H_{46}P_2PdO$: C, 61.74; H, 7.69. Found: C, 61.61; H, 7.79%.

*5.2.2. (dcpe)Pd(dba) (**2**)*

A solution of dcpe (817 mg, 1.93 mmol) in 10 ml C_6H_6 was added during 10 min to a stirred dark purple solution of $Pd_2(dba)_3{\cdot}CHCl_3$ in 15 ml C_6H_6. Within 5 min after the end of addition, a bright orange solid precipitated. After 1.25 h, the mixture was poured into 100 ml Et_2O and the crude orange product was collected by filtration and then crystallized from CH_2Cl_2–Et_2O at −20°C as dark orange–red cubes which were washed with pentane and dried in vacuo at 40°C for 16 h; yield 841 mg (57%). ^{1}H-NMR (toluene-d_8): δ 0.40–2.00 (m, 48, dcpe), 5.06 (br, 1, HC=CH), 5.55 (br, 1, HC=CH), 6.80–7.50 (m, 11, Ph and HC=CH), 7.70 (br, 1, HC=CH). ^{31}P{H}-NMR (toluene-d_8): δ 56.50 (br, 1), 58.37 (br, 1). Anal. Calc. for $C_{43}H_{62}OP_2Pd$: C, 67.66; H, 8.19. Found: C, 67.28; H, 8.38%.

*5.2.3. (dippe)Pd(Ph)Br (**3a**)*

An NMR tube was charged with **1** (38 mg, 0.06 mmol) and PhBr (49 mg, 0.32 mmol, five equivalents). 0.8 ml toluene-d_8 was condensed via vacuum transfer onto the mixture and the NMR tube was then flame-sealed. The resulting orange solution was kept at 65°C in an oil bath and monitored by ^{1}H- and ^{31}P{H}-NMR. After 5 days, the reaction was judged to be complete. ^{1}H-NMR (toluene-d_8): δ 0.72 (dd, 6, $CH(CH_3)_2$, J_{HP}=17, $J_{HH}=7$), 0.80 (dd, 6, $CH(CH_3)_2$, $J_{HP}=15$, $J_{HH}=7$), 0.94 (dd, 6, $CH(CH_3)_2$, $J_{HP}=13$, $J_{HH}=7$), 1.07 (m, 3, $CH(CH_3)_2$), 1.30 (m, 1, $CH(CH_3)_2$), 1.34 (dd, 6, $CH(CH_3)_2$, $J_{HP}=16$, $J_{HH}=7$), 1.81 (m, 2, PCH_2CH_2P), 2.19 (m, 2, PCH_2CH_2P), 6.87 (d, 2, free dba HC=CH, $J_{HH}=16$), 7.26 (m, 4, free dba Ph), 6.98 (m, 3), 7.41 (m, 6, free dba Ph), 7.62 (m, 2), 7.72 (d, 2, free dba HC=CH, $J_{HH}=16$), plus resonances for excess PhBr. ^{31}P{H}-NMR (toluene-d_8): δ 68.58 (d, 1, $J_{PP}=19$), 75.48 (d, 1).

*5.2.4. (dippe)Pd(Ph)I (**3b**)*

An NMR tube was charged with **1** (37 mg, 0.06 mmol) and PhI (63 mg, 0.31 mmol, five equivalents). 0.8 ml toluene-d_8 was condensed via vacuum transfer onto the mixture and the NMR tube was then flame-sealed. The resulting orange solution was kept at 65°C in an oil bath and monitored by ^{1}H- and ^{31}P{H}-NMR. After 72 h, **1** had been consumed completely. ^{1}H-NMR (toluene-d_8): δ 0.70 (dd, 6, $CH(CH_3)_2$, $J_{HP}=16$, $J_{HH}=7$), 0.78 (dd, 6, $CH(CH_3)_2$, $J_{HP}=15$, $J_{HH}=7$), 0.92 (dd, 6, $CH(CH_3)_2$, $J_{HP}=13$, $J_{HH}=7$), 1.25 (m, 1, $CH(CH_3)_2$), 1.10 (m, 3, $CH(CH_3)_2$), 1.32 (dd, 6, $CH(CH_3)_2$, $J_{HP}=16$, $J_{HH}=7$), 1.81 (m, 2, PCH_2CH_2P), 2.25 (m, 2, PCH_2CH_2P), 6.87 (d, 2, free dba HC=CH, $J_{HH}=16$), 6.89 (m, 3), 7.26 (m, 4, free dba Ph), 7.41 (m, 6, free dba Ph), 7.62 (m, 2), 7.72 (d, 2, free dba HC=CH, $J_{HH}=16$), plus resonances for excess PhI. ^{31}P{H}-NMR (toluene-d_8): δ 68.08 (d, 1, $J_{PP}=18$), 72.43 (d, 1).

5.3. Molecular mechanics calculations

Molecular mechanics calculations were performed on (dippe)Pd(dba) using the MM+ force field of HYPERCHEM 5.11. The geometry of the immediate coordination sphere of the complex (P_2PdC_2) was taken from the X-ray structure of **1** and kept frozen during all energy minimizations. A conformational energy surface was generated by systematically varying the torsional angles of the two independent C–C bonds to the carbonyl carbon, holding those angles fixed, and then performing an energy minimization. Both sets of angles were varied systematically from −180 to 180° in 30° increments. The resultant symmetric energy contour showed local energy minima corresponding to conformers I, II, and III, with the global minimum belonging to the *s-trans*, *s-trans* conformer I. The relative energies of I, II, and III were further refined by full geometry optimization (except for the frozen core) starting from the local minima of the conformational surface. The rotational barriers were estimated from the original conformational map and were not optimized.

5.4. X-ray crystallography

*5.4.1. Structure solution and refinement for (dippe)Pd(dba) (**1**)*

An orange column-like crystal of **1** of dimensions $0.66\times0.40\times0.36$ mm, obtained by slow diffusion of pentane into a benzene solution of the complex under Ar, was affixed to a thin glass fiber with epoxy cement. General procedures for crystal orientation, unit cell determination and refinement, and data collection on the Enraf–Nonius CAD4 diffractometer have been published [29]. Those specific to the present structure are presented in Table 1. The initial orthorhombic cell indicated by the CAD4 software was confirmed by the observation of *mmm* diffraction symmetry and the space group was uniquely determined by the systematic absences observed in the final data set. The intensity data was corrected for a linear 4.5% decay in the intensity monitors, for Lorentz and polarization effects, and an empirical absorption coefficient was applied by using ψ scans for several reflections with χ near 90°. The SHELXTL-PLUS v.5.1 software package (Bruker AXS; Madison, WI) was used to carry out the structure solution and refinement. The position of the Pd atom was determined from a sharpened Patterson function and the remainder of the structure was developed by successive cycles of full-matrix, least-squares refinement followed by calculation of a difference Fourier map. Hydrogen atoms were placed in calculated positions with riding contributions except for those bonded to C(15) and C(16) (coordinated double bond of dba) which were refined with isotropic displacement parameters.

*5.4.2. Structure solution and refinement for (dcpe)Pd(dba) (**2**)*

An orange block-like crystal of **2** of dimensions $0.33 \times 0.30 \times 0.26$ mm, obtained by cooling to -20°C a solution of the complex in CH_2Cl_2–Et_2O, was mounted into a thin-walled glass capillary which was then flame-sealed. General procedures for crystal orientation, unit cell determination and refinement, and data collection on the Enraf–Nonius CAD4 diffractometer are similar to those reported for **1**. Those specific to the present structure are presented in Table 1. The CAD4 software indicated a triclinic cell initially and no higher symmetry was found. The intensity statistics indicated a centrosymmetric space group and therefore $P\bar{1}$ was selected and confirmed as the correct space group by the successful refinement of the structure. The intensity data was corrected for a linear 4.3% decay in the intensity monitors, for Lorentz and polarization effects, and an empirical absorption coefficient was applied by using ψ scans for several reflections with χ near 90°. The SHELXTL-PLUS v.5.1 software package (Bruker AXS; Madison, WI) was used to carry out the structure solution and refinement. The position of the Pd atom was determined from a sharpened Patterson function and the remainder of the structure was developed by successive cycles of full-matrix, least-squares refinement followed by calculation of a difference Fourier map. Hydrogen atoms were placed in calculated positions with riding contributions except for those bonded to C(28) and C(29) (coordinated double bond of dba) which were refined with isotropic displacement parameters.

6. Supplementary material

Crystallographic data for the structural analysis have been deposited with the Cambridge Crystallographic Data Centre, CCDC nos. 143662 for compound **1** 143661 for compound **2**. Copies of this information may be obtained free of charge from: The Director, CCDC, 12 Union Road, Cambridge, CB2 1EZ, UK (Fax: +44-1223-336-033; e-mail: deposit@ccdc.cam.ac.uk or www: http://www.ccdc.cam.ac.uk).

Acknowledgements

Dow Corning corporation and the Tulane Center for Bioenvironmental Research (DSWA) are gratefully acknowledged for financial support of this work.

References

[1] L.S. Hegedus, in: M. Schlosser (Ed.), Organometallics in Synthesis, Wiley, New York, 1994, p. 383.
[2] M.F. Rettig, P.M. Maitlis, Inorg. Synth. 17 (1977) 134.
[3] T. Ukai, H. Kawazawa, Y. Ishii, J.J. Bonnett, J.A. Ibers, J. Organomet. Chem. 65 (1974) 253.
[4] C. Amatore, A. Jutand, Coord. Chem. Rev. 178–180 (1998) 511.
[5] C. Amatore, A. Jutand, G. Meyer, H. Atmani, F. Khalil, F.O. Chahdi, Organometallics 17 (1998) 2958.
[6] C. Amatore, A. Jutand, F. Khalil, M.A. M′Barki, L. Mottier, Organometallics 12 (1993) 3168.
[7] C. Amatore, G. Broeker, A. Jutand, F. Khalil, J. Am. Chem. Soc. 119 (1997) 5176.
[8] C.G. Pierpont, R.M. Buchanan, H.H. Downs, J. Organomet. Chem. 123 (1977) 103.
[9] T. Ito, Y. Takahashi, Y. Ishii, J. Chem. Soc. Chem. Commun. (1972) 629.
[10] W.A. Herrmann, W.R. Thiel, C. Brobmer, K. Öfele, J. Organomet. Chem. (1993) 461151.
[11] X. Bei, H.W. Turner, W.H. Weinberg, A.S. Guram, J. Org. Chem. 64 (1999) 6797.
[12] J. Fawcett, R.D.W. Kemmitt, D.R. Russell, O. Serindag, J. Organomet. Chem. 486 (1995) 171.
[13] W. Clegg, G.R. Eastham, M.R.J. Elsegood, R.P. Tooze, X.L. Wang, K. Whiston, Chem. Commun. (1999) 1877.
[14] K. Selvakumar, M. Valentini, M. Wörle, P.S. Pregosin, Organometallics 18 (1999) 1207.
[15] M. Tschoerner, G. Trabesinger, A. Albinati, P.S. Pregosin, Organometallics 16 (1997) 3447.
[16] A.D. Burrows, N. Choi, M. McPartlin, D.M.P. Mingos, S.V. Tarlton, R. Vilar, J. Organomet. Chem. 573 (1999) 313.
[17] J. Andrieu, P. Braunstein, A.D. Burrows, J. Chem. Research (S) (1993) 380.
[18] Y. Pan, J.T. Mague, M.J. Fink, J. Am. Chem. Soc. 115 (1993) 3842.
[19] M.C. Mazza, C.G. Pierpont, Inorg. Chem. 12 (1973) 2955.
[20] M.C. Mazza, C.G. Pierpont, J. Chem. Soc. Chem. Commun. (1973) 207.
[21] C.G. Pierpont, M.C. Mazza, Inorg. Chem. 13 (1974) 1891.
[22] R. Benn, P. Betz, R. Goddard, P.W. Jolly, N. Kokel, C. Krüger, I. Topalovic, Z. Naturforsch. Teil B 46 (1991) 1395.
[23] K.R. Pörschke, C. Pluta, B. Proft, F. Lutz, Z. Naturforsch. Teil B 48 (1993) 608.
[24] R. Benn, P.W. Jolly, T. Joswig, R. Mynott, K.-P. Schick, Z. Naturforsch. Teil B 41 (1986) 680.
[25] J. Krause, W. Bonrath, K.R. Pörschke, Organometallics 11 (1992) 1158.
[26] M. Tschoerner, P.S. Pregosin, Organometallics 18 (1999) 670.
[27] [(μ-dippe)Pd]$_2$, a convenient source of naked (dippe)Pd(0), inserts readily into the carbon–chlorine bond of PhCl at room temperature; results will be published elsewhere.
[28] M.D. Fryzuk, G.K.B. Clentsmith, S.J. Rettig, Organometallics 15 (1996) 2083.
[29] J.T. Mague, C.L. Lloyd, Organometallics 7 (1988) 983.